Computers & Fluids 39 (2010) 1332–1344

Contents lists available at ScienceDirect

Computers & Fluids

journal homepage: www.elsevier.com/locate/compfluid

Boundary formulations for high-order finite differences on staggered meshes

V.D. Topalian [a,*,1], J.B. Freund [a,b]

[a] Department of Mechanical Science and Engineering, University of Illinois at Urbana–Champaign, Urbana, IL 61801, USA
[b] Department of Aerospace Engineering, University of Illinois at Urbana–Champaign, Urbana, IL 61801, USA

ARTICLE INFO

Article history:
Received 2 April 2009
Received in revised form 3 January 2010
Accepted 3 April 2010
Available online 14 April 2010

Keywords:
Use boundary conditions
Staggered mesh
Compressible flows
Compact schemes
High-order methods

ABSTRACT

Discretizations of the compressible flow equations with flow variables defined at different staggered positions on a regular mesh have accuracy and stability advantages over standard collocated discretization, but implementation of boundary conditions is hampered without all flow variables available at any boundary point. Boundary schemes for implementation of the boundary conditions compatible with staggered mesh discretizations are considered in this study. We focus on a combination of fourth- and fifth-order schemes near the boundary that are stable when sixth-order centered schemes are used for the interior points. Characteristics-based formulations provide a physically meaningful treatment for all the variables, avoiding the use of extrapolation. However its application on staggered meshes has not been systematically studied and its implementation is unclear since this method requires collocation of all the variables at the boundary, which is not natural for standard staggered mesh formulations. We show that including all the flow variables at the boundary can be done in a way that does not affect resolution or accuracy of the formulation. Predictions based upon analysis with model equations are verified with a staggered mesh flow solver.

1. Introduction

The staggered mesh arrangement of variables was introduced for incompressible flows by Harlow and Welch [1]. This arrangement provides a robust formulation because of the discrete conservation of kinetic energy, in addition to mass and momentum [2]. Staggering also improves resolution [3], although this benefit applies only to the terms in the Navier–Stokes equations which do not need an intermediate or final interpolation operation [4]. A formulation for compressible flows was developed by Nagarajan et al. [5], where it was shown the superior stability properties over the regular and collocated grid formulation. Boersma [4] implemented this discretization successfully for cases that include chemical species transport and reaction.

The choice of boundary schemes and the treatment of boundary conditions for such formulations has received little attention. Regarding the boundary schemes, low-order schemes (third-order for the boundary point and fourth-order for the near-boundary point) have been used [4,5] for a sixth-order interior scheme. At boundaries, discrete conservation criteria and extrapolation of variables have been proposed [4,5], but not systematically studied.

Any physical boundary condition (e.g., no-slip, constant temperature) is inherently coupled with the discretization. In this study, we address both the use of higher-order discretizations at and near-boundary points and characteristics based formulation for the evolution of variables at the boundary.

1.1. Staggered mesh

Consider the discretization of a one-dimensional domain by a uniform mesh using $N+1$ points, so that the distance between points is $\Delta x = L/N$. The first point is at $x = 0$; the last point is at $x = L$. We call this the h-mesh. We define the midpoints of all adjacent points in the h-mesh to be the c-mesh. This mesh is thus staggered by $\Delta x/2$ relative to the h-mesh. In problems with more than one variable it can be advantageous to define different variables on the different meshes. For flow simulations, is common to define the velocity (or the mass-flux) on the h-mesh, and the pressure, density, and other thermodynamic variables on the c-mesh, as shown in Fig. 1.

In our c-mesh we also include the boundary points since most physical boundary conditions require at least one thermodynamic variable on the boundary. Note that this is not true for incompressible flows, since the pressure field is completely determined by the velocity field. For compressible flows, having this point allows us to

* Corresponding author. Tel.: +1 217 2442008; fax: +1 217 3331910.
E-mail addresses: topalian@illinois.edu (V.D. Topalian), jbfreund@illinois.edu (J.B. Freund).
[1] Present address: Department of Computational Science and Engineering, University of Illinois at Urbana–Champaign, 2270 DCL, 1304 West Springfield Avenue, Urbana, IL 61801, USA.

0045-7930/$ - see front matter © 2010 Elsevier Ltd. All rights reserved.
doi:10.1016/j.compfluid.2010.04.003

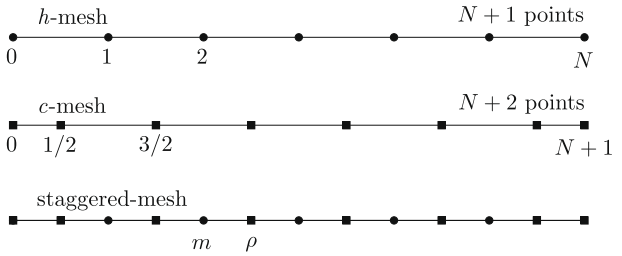

Fig. 1. Staggered mesh in one dimension.

set a variable's value at the boundary according to a problem's specification, in cases to compute it at the boundary in terms of other variables, or to time advance an auxiliary boundary equation for its evolution. These different cases are needed for different physical conditions and are discussed further throughout this paper. Often in formulations the values are unphysically extrapolated as needed from the interior points [4]. We also evaluate this option.

1.2. Discrete operators

We define our discrete interpolation or differentiation operators as mappings that either map to the same mesh where the data is defined or from one mesh to the other. We write these operators in matrix form as

$$\mathbf{M}\delta^p\boldsymbol{f} = \mathbf{D}\boldsymbol{f},$$

where $\delta^p\boldsymbol{f}$ is the pth derivative of $\boldsymbol{f}$. For finite differences, if the schemes are explicit, $\mathbf{M}$ is the identity matrix. For so-called compact schemes (e.g., [3]), $\mathbf{M}$ is a banded matrix, which is inverted to solve for $\delta^p\boldsymbol{f}$:

$$\delta^p\boldsymbol{f} = \mathbf{M}^{-1}\mathbf{D}\boldsymbol{f}.$$

The resulting matrix $\mathbf{C} = \mathbf{M}^{-1}\mathbf{D}$ is typically full, so in practice the stencil information is, of course, stored in terms of $\mathbf{M}$ and $\mathbf{D}$. Note that $\mathbf{C}$ is not a square matrix when mapping between meshes. For example, if $\boldsymbol{f}$ is defined on the c-mesh and $\delta^p\boldsymbol{f}$ on the h-mesh, then $\mathbf{C}$ is an $(N+1)\times(N+2)$ matrix. We consider mainly mappings from one mesh to the other, which are used to solve flow or similar equations on staggered meshes.

Away from any boundary, a general expression for implicit centered schemes that compute a result on an h-mesh from data on a c-mesh is

$$\delta^p f_i + \sum_{j=1}^{w}\alpha_j(\delta^p f_{i+j} + \delta^p f_{i-j}) = \sum_{j=1}^{w'}\frac{a_{j-1/2}}{(\Delta x)^p}(f_{i+(j-1/2)} - f_{i-(j-1/2)}). \tag{1}$$

The coefficients α_j and a_j are often chosen to maximize the order of accuracy, though this can be relaxed to tailor the resolution of the scheme [3,6].

For the boundary and near-boundary points, special sided schemes need to be considered. The general form of these is

$$\delta^p f_i + \sum_{j\neq i}\alpha_{ij}\delta^p f_j = \sum_k \frac{a_{ik}}{(\Delta x)^p} f_k.$$

The coefficients for the specific interpolation and first-derivative operators we use in our examples are given in Appendix A and were optimized for order of accuracy.

For convenience, we rename the computed values of interpolation ($\delta^0\boldsymbol{f}\to\boldsymbol{\zeta f}$) and first-derivative ($\delta^1\boldsymbol{f}\to\boldsymbol{\delta f}$) and add to them as subscript h or c corresponding to the mesh on which they are calculated (their target mesh). We also add subscripts to the matrices $\mathbf{M}$ and $\mathbf{D}$ indicating the order of the derivative they represent and the mesh onto which the result is mapped. For example, the equation for mapping the first-derivative of data on the h-mesh onto the c-mesh is $\mathbf{M}_{1c}(\delta_c\boldsymbol{f}) = \mathbf{D}_{1c}\boldsymbol{f}$. Similarly, for interpolation to the h-mesh we have $\mathbf{M}_{0h}(\zeta_h\boldsymbol{f}) = \mathbf{D}_{0h}\boldsymbol{f}$.

Our analysis is on uniform meshes. Standard mapping methods can be used to extend to non-uniform meshes.

1.3. Motivation for the model equations

Consider the compressible flow equations,

$$\frac{\partial\rho}{\partial t} + \frac{\partial m_i}{\partial x_i} = 0,$$
$$\frac{\partial m_i}{\partial t} + \frac{\partial u_j m_i}{\partial x_j} + \frac{\partial p}{\partial x_i} = \frac{\partial\tau_{ij}}{\partial x_j},$$
$$\frac{\partial\rho e}{\partial t} + \frac{\partial u_j\rho e}{\partial x_j} + p\frac{\partial u_j}{\partial x_j} = \tau_{ij}\frac{\partial u_i}{\partial x_j} - \frac{\partial q_j}{\partial x_j},$$

where the viscous stress is $\tau_{ij} = \mu(u_{i,j} + u_{j,i} - (2/3)u_{k,k}\delta_{ij})$, the mass-flux is $m_i = \rho u_i$, the viscosity is $\mu = \mu_0(T/T_0)^{0.76}$, and heat flux is $q_j = -\kappa T_j$. The thermodynamic relation $\rho e = p/(\gamma-1)$ and state equation $p = \rho R\,T$ are as for a perfect gas. As written, the independent variables are ρ, m_i and ρe (density, momentum and internal energy). For analysis of the discretization, we consider for now the one-dimensional version of the Euler equations for isentropic flow,

$$\frac{\partial\rho}{\partial t} + \left(\frac{\partial m}{\partial x}\right)_{\mathrm{I}} = 0,$$
$$\frac{\partial m}{\partial t} + \left(\frac{\partial um}{\partial x}\right)_{\mathrm{II}} + \left(\frac{\partial p}{\partial x}\right)_{\mathrm{III}} = 0. \tag{2}$$

On collocated meshes it is natural to use the same derivative operator for all the terms in (2). However, on staggered meshes with the density stored on the c-mesh and momentum on the h-mesh, different operators are needed for the different terms. For term II, for example, we need to first compute the value of um on the c-mesh using interpolation, and then compute the derivative. A simpler hyperbolic equation, which requires a similar treatment, is $\partial_t v + \partial_x v = 0$. This is our model Eq. (1) (ME1). On the other hand it is natural to evaluate terms I and III using staggered derivative operators without interpolation. In this case, a simpler hyperbolic system, which requires the same operators, is $\partial_t\ p + \partial_x u = 0$, $\partial_t u + \partial_x p = 0$, with u on the h-mesh and p on the c-mesh. This is our model Eq. (2) (ME2). We expect that the discrete properties for the model equations will translate when the same operators are used for the Navier–Stokes (NS) equations.

1.4. Criteria for the construction of boundary schemes

We focus on the case in which sixth-order schemes are used for interpolation and differentiation at interior points. These high-order schemes with different boundary closures were already implemented on staggered meshes [5,4]. For this stencil, $w = 1$ and $w' = 2$ in (1). Different schemes for the boundary and near-boundary points ($c_0, c_{1/2}, h_0$ and h_1) are therefore needed. There are several ways to construct boundary schemes of a given order. Ours, specified in Tables 9–16, satisfy these conditions:

1. The schemes are optimized by order of accuracy and the nearest points are used to construct them.
2. The tridiagonal structure of the $\mathbf{M}$ matrix is preserved.
3. Only implicit schemes for the near-boundary points are considered.
4. Both implicit and explicit schemes are considered for boundary points.

Schemes that make use of ('a' cases) and do not make use of ('b' cases) the boundary points on the *c*-mesh are also considered. These schemes are designated as follows:

1. The first letter and the first number indicates the point to which the scheme applies.
2. The second number is the formal order of the scheme.
3. The following letter specifies whether the scheme is implicit (i) or explicit (e).
4. For the first-derivative schemes, the last letter indicates if it uses the boundary point of the *c*-mesh ('a') or not ('b'). This last letter is omitted if this distinction does not apply.

For example, c15ia is an implicit fifth-order scheme for a near-boundary point of the *c*-mesh which uses the derivative (and functional value) at the boundary point.

There are clearly many ways in which these schemes can be combined to close an operator. The ones we tested are summarized in Table 1, with the closure schemes grouped by their order of accuracy. The cases considered are then: (1) combination of third and fourth-order closures for the boundary and the near-boundary point; (2) fifth-order schemes for both; and (3) sixth-order schemes for both. Only type 'a' schemes (with boundary points) are considered here, because we are interested in evaluating the effect of the extra point on the resolution.

In Section 2, we assess the resolution properties of these schemes by two methods: first by using a test function and second by solving the semi-discrete version of the model equations ME1 and ME2. The first method is a simpler way to assess resolution, and allows us to evaluate each interpolation and derivative operator separately. The second method is, as proposed by Kwok et al. [7], for evaluating resolution of different formulations in bounded domains. As it will be shown, the resolution results obtained by the second method are similar to those obtained considering the L_∞-norm in the first method.

In Section 3, the performance of different strategies to implement the boundary conditions is assessed when the model problems are marched in time. It is seen that the characteristics method is unstable in the inviscid limit. However, it is also shown that a small amount of physical viscosity, of the kind naturally present even in fairly high Reynolds number NS simulations, makes the system stable and accurate. It is also seen that the use of the extra point in the *c*-mesh, which facilitates the application of physical boundary conditions, little affects the accuracy of the results.

2. Resolution properties of the discrete operators

2.1. Boundary effects

In finite differences, the resolution of the sided schemes used at and near-boundaries is poorer than the one for centered schemes.

Table 1
Case definitions for resolution tests.

		Boundary	Schemes	
	c_0	$c_{1/2}$	h_0	h_1
Interpolation				
1	$=h_0$	c14e	$=c_0$	h14i
2	$=h_0$	c15i	$=c_0$	h15i
3	$=h_0$	c16i	$=c_0$	h16i
Derivative				
1	c03ea	c13e	h03ea	h14i
2	c05ia	c15ia	h05ia	h15ia

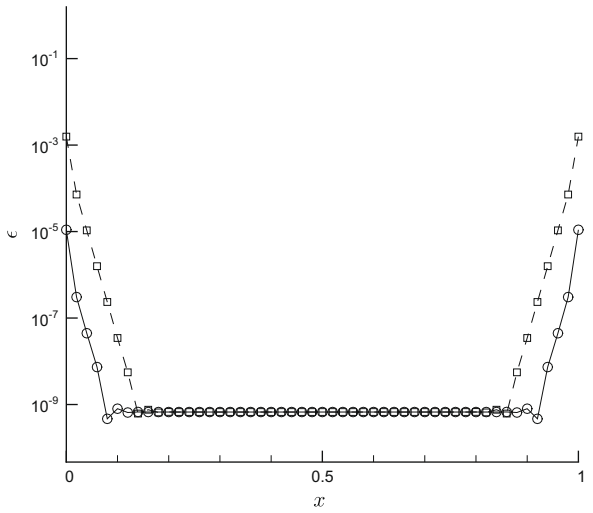

Fig. 2. Modulus of the error for each point in x for closures ∘ h03ib-h14i and □ h04ea-h15ia defined in Tables 13 and 14 for the derivative on the h-mesh of (6), with $N = 50$ and $k = 2\pi$.

This translates into greater (usually several orders of magnitude) errors near the boundaries. For implicit schemes, the error is spread to nearby points, as it is shown in Fig. 2 where it is seen also that it decays exponentially to the error of the interior scheme.

An estimate of this exponential decay rate can be obtained. If we consider a periodic function, then $\delta f_j = k' f_j$, where k' is the modified wavenumber of the scheme. Then, the error at point j is $\epsilon_j = \delta f_j - f'_j = |(k' - k) f_j| = |(k' - k)/k|$. This solution of δf satisfies

$$\alpha \delta f_{j-1} + \delta f_j + \alpha \delta f_{j+1} = \mathrm{rhs}_j. \tag{3}$$

For a nonperiodic domain, close to the boundary, we assume that the approximated value is

$$\delta f_j = k' f_j + \theta_j, \tag{4}$$

where θ_j is the additional error introduced by the boundary scheme. For point 1, (3) gives

$$\alpha \delta f_0 + \delta f_1 + \alpha \delta f_2 = \mathrm{rhs}_1,$$

which upon substitution of (4) is

$$k'(\alpha f_0 + f_1 + \alpha f_2) + (\alpha \theta_0 + \theta_1 + \alpha \theta_2) = \mathrm{rhs}_1,$$

so,

$$\alpha \theta_0 + \theta_1 + \alpha \theta_2 = 0.$$

If we assume that $\theta_2 \ll \theta_1$, which is expected since stencils near the boundary are lower-order and thus typically less accurate, the additional error at point 1 is $\theta_1 = -\alpha \theta_0$. In the same way, $\theta_2 = -\alpha \theta_1 = \alpha^2 \theta_0$. We can use this value of θ_2 to correct the value of θ_1, which gives $\theta_1 = (-\alpha - \alpha^3)\theta_0$. In general,

$$\theta_j = (-\alpha - \alpha^3)^j \theta_0 + o(\alpha^{3j}). \tag{5}$$

This result is independent of whether the operator is for a collocated or a staggered mesh. As an example, consider a fourth-order implicit scheme for the derivative on a collocated mesh, for which $\alpha = 1/4$. Fig. 3 compares the test case and the computed error, where we considered $\epsilon_0 \approx \theta_0$ and estimated the error as $\epsilon_j = -(k' - k) f_j + \theta_j -$.

Note that this estimate depends upon θ_j dominating for small j and the $k' \approx k$ difference dominating for large j. When both terms are of the same order, the approximation does not hold.

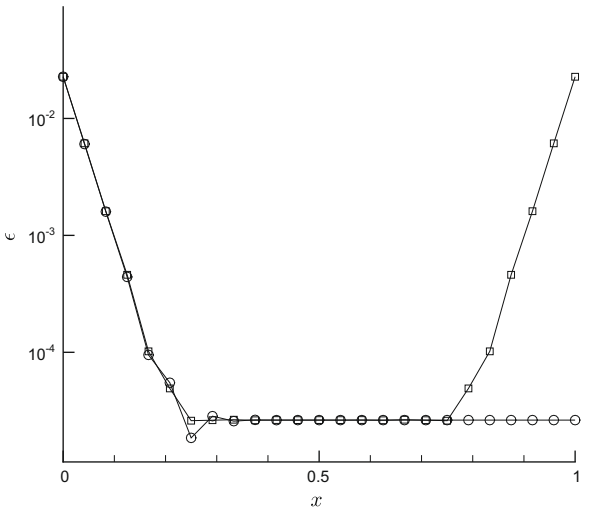

Fig. 3. Exponential error decay and modified wavenumber error: □ computed and ○ estimated.

2.2. Application of the operator to a test function

The test function we use is

$$f(x) = \frac{\exp(\mathrm{i}kx)}{(\mathrm{i}k)^p}, \tag{6}$$

where p is the order of the derivative of the mapping operator.

The resolution results are presented in terms of k/k_{max}, where $k_{max} = N\pi/L$ is the maximum wavenumber supported by the mesh. The relation to points per wavelength (ppw) is given by $k/k_{max} = 2/\text{ppw}$. Note that the L_2 error depends on the number of points used. Then, the L_∞ error is more meaningful in this case.

The specific schemes used in each case are summarized in Table 1. The results are shown in Figs. 4–7, where it is seen that higher-order closures lead to higher accuracy for most of the wavenumbers, specially as the problem becomes better resolved. The order of accuracy is not degraded by the use of the extra point. It is also seen that for ill-resolved features, the actual error is greater for higher-order schemes than for lower-order schemes.

A sometimes more useful resolution criterion is the fraction of wavenumbers with error lower than any particular value. In Table 2 we present this wavenumber fraction for errors of (0.1%, 1% and 10%).

As explained before, in applications sometimes a combination of two operators is needed, such as for term II in (2). This is done by interpolating m to the c-mesh and the differentiating mu back to the h-mesh. It is also possible to interpolate ρ to the h-mesh, computing um_x and obtaining its derivative using a collocated derivative operator. However, this option is not evaluated because it involves also the use of two operators, but one is for collocated meshes.

The resolution properties of this combined operator is shown in Table 3. It is seen that when the order of the derivative schemes is the same as that of the interpolation scheme the values for the derivative operator on the c-mesh are nearly the same as those of the derivative operator applied directly. In the case of the derivative operator to the h-mesh the resolution is more degraded for the schemes used.

2.3. Resolution by solution of the semi-discrete system

2.3.1. First-order wave equation

As mentioned in Section 1.3 the advection equation (ME1),

$$\frac{\partial v}{\partial t} + \frac{\partial v}{\partial x} = 0, \tag{7}$$

is a good model for term II in (2). We take $x \geqslant 0$ and assume $v = V(x)T(t)$, with $T(t) = \exp(-\mathrm{i}kt)$, so that the semi-discrete version is

$$\frac{\partial V}{\partial x} = \mathrm{i}kV. \tag{8}$$

The boundary condition $V(0) = 1$ gives exact solution $V = \exp(\mathrm{i}kx)$. As discussed for Navier–Stokes solutions, a combined staggered interpolation and derivative is needed, so the system of equations to solve is

$$(-\mathrm{i}k\mathbf{I} + \mathbf{C}_{1c}\mathbf{C}_{0h})\boldsymbol{V} = 0, \tag{9}$$

where V is the vector of function values at the h-mesh points. To enforce the boundary condition at $x = 0$, the first row of this system (the equation for V_0) is replaced by $V_0 = 1$. Note that for this model equation, this boundary condition also determines the value of the derivative at the boundary, since $(\mathrm{d}V/\mathrm{d}x)_{-0} = \mathrm{i}kV_0 = \mathrm{i}k$. Kwok et al. [7] made use of this fact. However, this is not true when the Navier–Stokes equations are solved. For this reason, in our approach the first derivative at point c_0 is approximated using a one-sided scheme. The discrete system (9) is equivalent to the block-matrix system:

$$\begin{pmatrix} -\mathrm{i}k\mathbf{I} & \mathbf{I} & \mathbf{0} \\ \mathbf{0} & \mathbf{M}_{1c} & -\mathbf{D}_{1c} \\ -\mathbf{D}_{0h} & \mathbf{0} & \mathbf{M}_{0h} \end{pmatrix} \begin{pmatrix} \boldsymbol{V} \\ \delta_c \boldsymbol{V} \\ \xi_h \boldsymbol{V} \end{pmatrix} = \begin{pmatrix} \boldsymbol{0} \\ \boldsymbol{0} \\ \boldsymbol{0} \end{pmatrix},$$

where again the equation for point V_0 (first row of the first block) is replaced by the boundary condition $V_0 = 1$, and where the

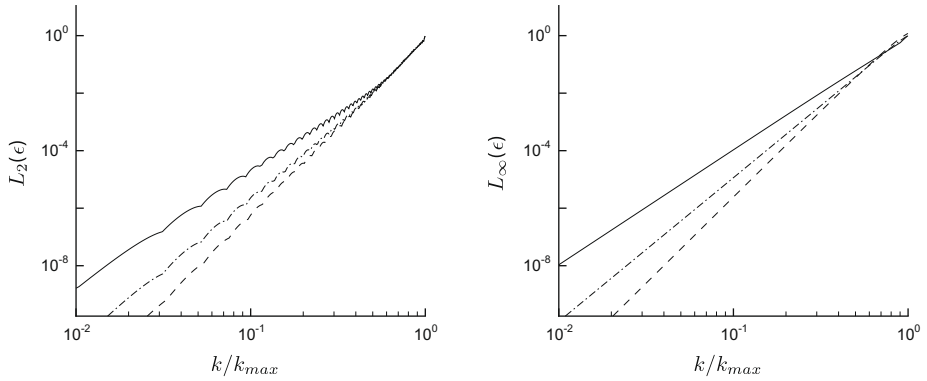

Fig. 4. Resolution for interpolation to the h-mesh (considering the boundary points in the c-mesh) for closures 1 —, 2 -·- and 3 ----.

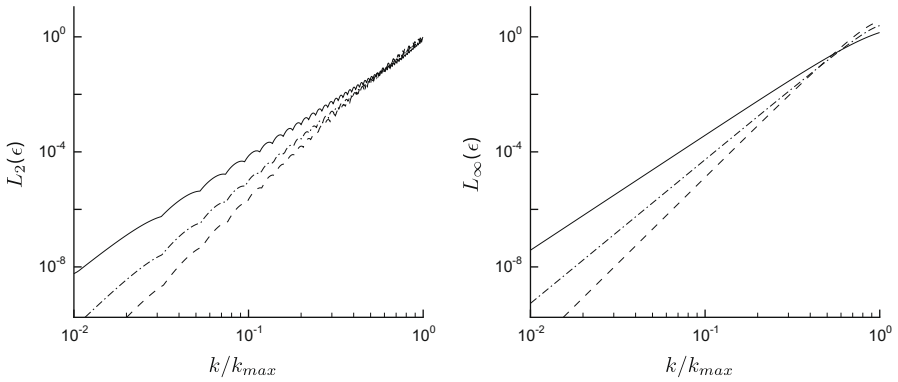

Fig. 5. Resolution for interpolation to the *c*-mesh (considering the boundary points in the *c*-mesh) for closures 1 —, 2 -·- and 3 ----.

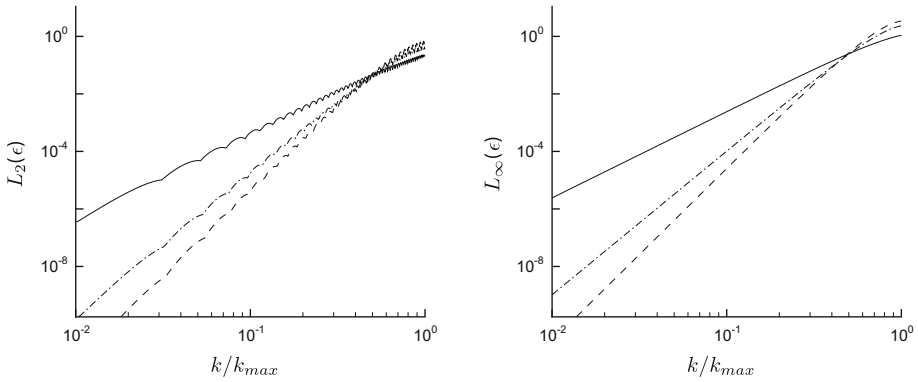

Fig. 6. Resolution for first-derivative to the *h*-mesh (considering the boundary points in the *c*-mesh) for closures 1 —, 2 -·- and 3 ----.

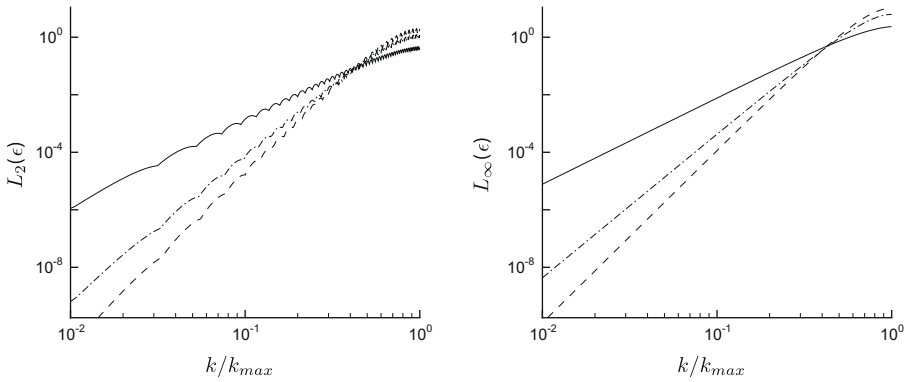

Fig. 7. Resolution for first-derivative to the *c*-mesh (considering the boundary points in the *c*-mesh) for closures 1 —, 2 -·- and 3 ----.

interpolation to the *h*-mesh and the derivative mapped back to the *c*-mesh ($\xi_h \boldsymbol{V}$ and $\delta_c \boldsymbol{V}$, respectively) are unknowns. The corresponding equations for the *h*-mesh is obtained by changing mesh subscripts *c* and *h* in the above systems. In both cases, the system is solved and compared to the exact solution to evaluate the scheme.

Results from this test are shown in Fig. 8, and Table 4 shows the wavenumber fraction for errors of 0.1%, 1% and 10%. Note that the L_2-norm of the error obtained by this method for ME1 is similar to the L_∞-norm of the error obtained by application of a test function to the combined operators (results in Tables 3 and 4). This is because the error is dominated by that of the boundary scheme, and in this case, when the solution of the model problem is sought, the error at the boundary affects most of the domain.

2.3.2. Second-order wave equation

A system of first-order equations (ME2),

$$\frac{\partial p}{\partial t}+\frac{\partial u}{\partial x}=0, \qquad \frac{\partial u}{\partial t}+\frac{\partial p}{\partial x}=0, \tag{10}$$

serves as our model for terms I and III in (2), with u defined on the *h*-mesh and p defined on the *c*-mesh. These equations, unlike ME1, can be marched in time by just using only the staggered derivative operators, without need for interpolation.

At a boundary, (10) can be written in terms of incoming and outgoing characteristics as

$$\frac{\partial p}{\partial t}+\frac{\mathscr{L}_1+\mathscr{L}_2}{2}=0, \quad \frac{\partial u}{\partial t}+\frac{\mathscr{L}_1-\mathscr{L}_2}{2}=0, \tag{11}$$

Table 2
Resolution of interpolation and derivative operators.

		L_2			L_∞		
Operator	Closure	0.1%	1%	10%	0.1%	1%	10%
ζ_h	1	0.26	0.47	0.72	0.17	0.31	0.57
	2	0.33	0.50	0.73	0.25	0.39	0.61
	3	0.34	0.51	0.72	0.27	0.41	0.60
ζ_c	1	0.19	0.35	0.65	0.13	0.23	0.42
	2	0.25	0.40	0.64	0.18	0.29	0.46
	3	0.28	0.41	0.61	0.21	0.31	0.46
δ_h	1	0.14	0.29	0.66	0.07	0.16	0.36
	2	0.23	0.36	0.60	0.16	0.25	0.41
	3	0.25	0.37	0.57	0.19	0.28	0.42
δ_c	1	0.09	0.19	0.44	0.05	0.11	0.24
	2	0.17	0.28	0.43	0.12	0.19	0.31
	3	0.19	0.29	0.44	0.15	0.21	0.32

Table 3
Resolution of combined operators.

		L_2			L_∞		
Operator	Closure	0.1%	1%	10%	0.1%	1%	10%
$\delta_h\zeta_c$	1	0.10	0.19	0.44	0.05	0.11	0.25
	2	0.15	0.27	0.46	0.10	0.18	0.31
	3	0.18	0.29	0.45	0.13	0.21	0.33
$\delta_c\zeta_h$	1	0.09	0.21	0.46	0.05	0.12	0.25
	2	0.17	0.28	0.46	0.12	0.20	0.32
	3	0.20	0.30	0.46	0.15	0.22	0.33

where $\mathscr{L}_1 = \lambda_1\partial_x(p+u)$ and $\mathscr{L}_2 = \lambda_2\partial_x(p-u)$, with $\lambda_1 = 1$ and $\lambda_2 = -1$. The semi-discrete version of (10), is obtained by taking $p(x,t) = P(x)\exp(-ikt)$ and $u(x,t) = U(x)\exp(-ikt)$, so that

$$\frac{\partial P}{\partial x} = ikU, \quad \frac{\partial U}{\partial x} = ikP. \tag{12}$$

The solution to this equation is $P(x) = c_1\exp(ikx) + c_2\exp(-ikx)$ and $U(x) = c_1\exp(ikx) - c_2\exp(-ikx)$, which we close by setting $u(0,t) = \exp(-ikt)$, which corresponds to $U(0) = 1$. At the right boundary we impose a non-reflecting condition $\mathscr{L}_2|_{x=1} = 0$, which fixes $c_1 = 1$ and $c_2 = 0$.

To evaluate resolution using this model equation, we consider the discretized version of (12). The resulting system, without consideration of boundary conditions is:

1. for interior points,

$$(-ikP + \delta_c U = 0)_{0<x<1},$$
$$(-ikU + \delta_h P = 0)_{0<x<1},$$

Table 4
Resolution by solution of the semi-discrete equation at c-mesh and h-mesh.

L_2	V_c			V_h		
Closure	0.1%	1%	10%	0.1%	1%	10%
1	0.07	0.14	0.28	0.07	0.14	0.21
2	0.17	0.25	0.36	0.10	0.16	0.26
3	0.18	0.27	0.38	0.13	0.18	0.28

2. for boundary points,

$$\left(-ikP + \frac{\mathscr{L}_1 + \mathscr{L}_2}{2} = 0\right)_{x=0,1},$$
$$\left(-ikU + \frac{\mathscr{L}_1 - \mathscr{L}_2}{2} = 0\right)_{x=0,1},$$

3. for the outgoing characteristics ($\mathscr{L}_1|_{x=1}$ and $\mathscr{L}_2|_{x=0}$) at the boundary points,

$$(\mathscr{L}_2 + \delta_h P - \delta_c U = 0)_{x=0},$$
$$(\mathscr{L}_1 - \delta_h P - \delta_c U = 0)_{x=1},$$

4. and for mapping the first-derivative at all points,

$$\mathbf{M}_{1h}\delta_h\boldsymbol{P} - \mathbf{D}_{1h}\boldsymbol{P} = \boldsymbol{0},$$
$$\mathbf{M}_{1c}\delta_c\boldsymbol{U} - \mathbf{D}_{1c}\boldsymbol{U} = \boldsymbol{0}.$$

To close the system, the equations for the incoming characteristics are obtained from the boundary conditions: taking $U|_{x=0} = 1$ yields $\mathscr{L}_1|_{x=0} = \mathscr{L}_2|_{x=0} + 2ik$. Doing this is equivalent to the procedure of the NSCBC method using the LODI relations [8]. The L_2-norm of the error for both U and P is shown in Fig. 9 as a function of the wavenumber for different closures. The resolution results are summarized in Table 5.

The values obtained in this case are similar to those obtained by analyzing the first-order wave equation (Table 4). The resolution curves in all cases show a wavy behavior (Figs. 8 and 9). The wavy behavior becomes more marked as the wavenumber increases, reaching order 1 spikes by $k/k_{max} = 0.4$, which corresponds to 5 points per wavelength. Again, the resolution is improved as higher-order closure schemes are used. More importantly, this analysis shows that the resolution of the overall system is not hurt by the characteristic treatment of the boundary points.

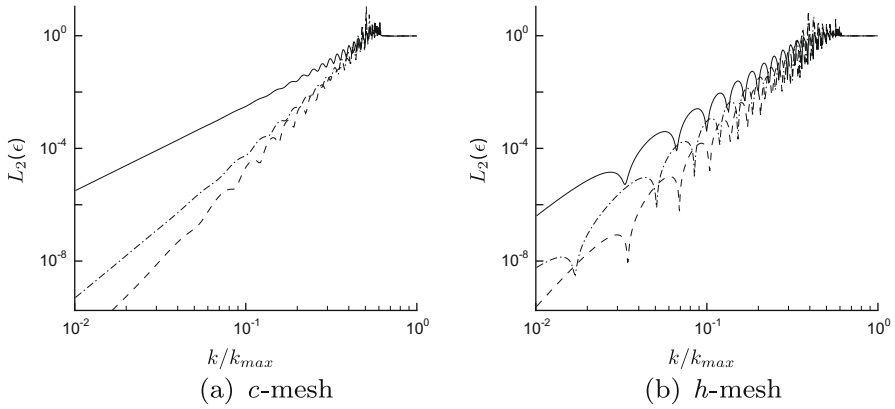

Fig. 8. Resolution by solution of the semi-discrete equation at (a) c-mesh and (b) h-mesh.

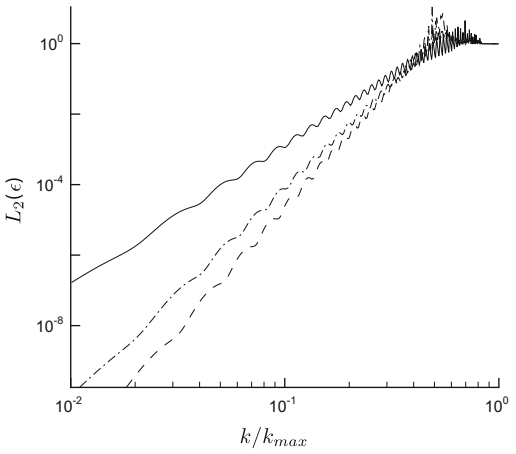

Fig. 9. Resolution by solution of the semi-discrete equation for mapping to a different mesh.

Table 5
Resolution by solution of the semi-discrete equation for mapping to a different mesh.

L_2	P_c			U_h		
Closure	0.1%	1%	10%	0.1%	1%	10%
1	0.09	0.17	0.29	0.09	0.17	0.29
2	0.15	0.22	0.32	0.15	0.22	0.32
3	0.17	0.25	0.34	0.17	0.25	0.34

3. Time marching accuracy and stability

3.1. Model Eq. (1)

In the first test, we march ME1 (7) in time using a fourth-order Runge–Kutta method (RK4) with initial condition

$$v(x,0) = \exp\left[-128\left(x-\frac{1}{2}\right)^2\right],$$

which should propagate unchanged to the right. The CFL number is $\mathrm{CFL} = \frac{c\Delta t}{\Delta x} = 0.1$, with $c = 1$ in this case. The results obtained by using CFL = 0.05 are indistinguishable, which confirms that the errors are dominated by the spatial discretization. At the left boundary, $v = 0$.

The scheme combinations tested are summarized in Table 6 for $N = 40$ and $N = 200$ points. Cases 1b, 2b and 3b do not use the boundary points on the c-mesh. Cases 1b and 2b are lower-order closures. Cases 1a and 2a are higher-order closures and make use of the boundary point. The difference between them is that 1a uses an explicit scheme for the boundary point and 2a uses an implicit scheme.

The results are shown in Fig. 10, where the energy in the domain is plotted against time. The energy that remains in the domain after the pulse exits is a measure of how well the boundary schemes perform: the higher the energy, the higher the spurious reflection produced by these schemes [9]. It is seen that as expected higher-order closures lead to better overall results as the problem becomes better resolved. More notably, it is also seen that schemes that use the extra point perform better than the ones that do not take it into account.

The test was also conducted for the case when the data is on the c-mesh for $N = 40$ and $N = 200$ results, and the results are shown in Fig. 11. In this case only boundary closures of type 'a' are considered (Table 7), because it is unclear how to implement the boundary condition at the left boundary if the c mesh point is not defined there. This issue will be considered in Section 3.2, when the tests are conducted on ME2.

The formulation works well for both closures tested, and the errors are of the same order as those of the previous case tested.

This test shows that the consideration of schemes with the extra point do not hurt the resolution properties of the formulation when the problem is marched in time. In fact, the results are slightly improved using this strategy.

Table 6
Closures for interpolation (c points) and derivative (h points) operators for the time marched test of model Eq. (1) on h-mesh.

		Boundary	Schemes	
Case name	c_0	$c_{1/2}$	h_0	h_1
1a	$=h_0$	c14e	h04ea	h15ia
2a	$=h_0$	c14e	h04ia	h15ia
1b	Not used	c14e	h03eb	h14ib
2b	Not used	c14e	h03ib	h14ib
3b	Not used	c14e	h04ib	h15ib

3.2. Tie into Navier–Stokes

When simulating flow with wall boundaries (no-slip, injecting, etc.) special considerations are needed. For example, consider an injecting isothermal wall, where the injection is a fixed momentum-flux. The density and the internal energy, which are unknown at the wall, are related by $\rho e = \rho T/(\gamma(\gamma-1))$. To close the system, we need an equation or a value for (say) ρ. We have several choices for determining (ρ) at the boundary: (1) extrapolate the value of density from the interior to the boundary, (2) march ρ in time using the original conservation equation, and (3) employ an evolution equation for ρ in terms of amplitudes of incoming and outgoing one-dimensional characteristics, but it is unclear a priori which strategy performs better. The following tests are designed to assess the relative merits of the different approaches. Note that this is particularly important in the case of an injecting wall, since the value of density at the boundary determines also the value of velocity at the boundary.

We evaluate these strategies using ME2 with Dirichlet conditions on u on both boundaries. As formulated the value of p is not actually needed at the boundary, though it is for an injecting wall. So in this case we have the choice also of not considering p at the boundary, which is straightforward to do when staggered meshes are used. With the aim of comparing the effects on accuracy of the different strategies that can be used for this problem, we consider the following cases:

1. p is not considered at the boundary (boundary discretization from Table 8, case 3b).
2. A value for p is extrapolated from the interior points (boundary discretization from Table 8, case 1a).
3. p is advanced in time using the original equation (boundary discretization from Table 8, case 1a).
4. p is advanced in time using the characteristic equation (boundary discretization from Table 8, case 1a).

The initial condition is a Gaussian pulse for both variables,

$$p(x,0) = u(x,0) = \exp\left(-128\left(x-\frac{1}{2}\right)^2\right),$$

which should bounce back and forth in the domain indefinitely. As this test is constructed, the pulse returns to its initial position after every non-dimensional time unit. At those times the solution is compared with the exact one, and the L_2 norm of the error is plotted against time in Fig. 12.

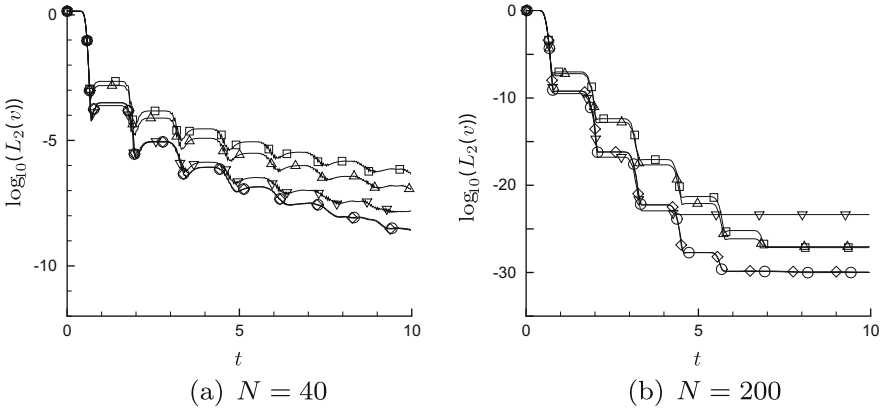

Fig. 10. Energy left in the computational domain as a function of time for data in h-mesh for (a) $N = 40$ and (b) $N = 200$ for the closure cases in Table 8: □, 1b; △, 2b; ▽, 3b; ♦, 1a; ○, 2a.

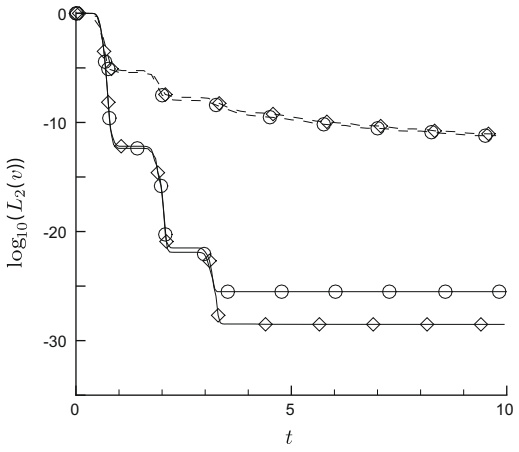

Fig. 11. Energy left in the computational domain as a function of time for data in c-mesh for $N = 40$ ---- and $N = 200$ — for the closure cases in Table 8: ♦, 1a; ○, 2a.

Table 7
Closures for interpolation (h points) and derivative (c points) operators for the time marched test of model Eq. (1) on c-mesh.

		Boundary	Schemes	
Case name	c_0	$c_{1/2}$	h_0	h_1
1a	c04ea	c15ia	$=c_0$	h14i
2a	c04ia	c15ia	$=c_0$	h14i

Table 8
Closures for the derivative operator for time marched tests.

		Boundary	Schemes	
Case name	c_0	$c_{1/2}$	h_0	h_1
1a	c04ea	c15ia	h04ea	h15ia
3b	not defined	c15ib	h04ib	h15ib

Table 9
Coefficients for sixth-order compact schemes at interior points.

Operator	w	w'	α_1	$a_{1/2}$	$a_{3/2}$
Interpolation	1	2	$\frac{3}{10}$	$\frac{3}{4}$	$\frac{1}{20}$
First-derivative	1	2	$\frac{9}{62}$	$\frac{63}{62}$	$\frac{17}{186}$

Table 10
Closure schemes for interpolation at the h-mesh for point $i = 0$.

Order	Name	α_{i0}	α_{i1}	$a_{i1/2}$	$a_{i3/2}$	$a_{i5/2}$	$a_{i7/2}$
3	h03eb	1		$\frac{15}{8}$	$-\frac{5}{4}$	$\frac{3}{8}$	
4	h04eb	1		$\frac{35}{16}$	$-\frac{35}{16}$	$\frac{21}{16}$	$-\frac{5}{16}$
4	h04ib	1	5	$\frac{15}{4}$	$\frac{5}{2}$	$-\frac{1}{4}$	
5	h05ib	1	7	$\frac{35}{8}$	$\frac{35}{8}$	$-\frac{7}{8}$	$\frac{1}{8}$

Table 11
Closure schemes for interpolation at the h-mesh for point $i = 1$.

Order	Name	α_{i0}	α_{i1}	α_{i2}	$a_{i1/2}$	$a_{i3/2}$	$a_{i5/2}$	$a_{i7/2}$
4	h14i	$\frac{1}{6}$	1	$\frac{1}{6}$	$\frac{2}{3}$	$\frac{2}{3}$		
5	h15i	$\frac{1}{10}$	1	$\frac{1}{2}$	$\frac{1}{2}$	1	$\frac{1}{10}$	
6	h16i	$\frac{1}{14}$	1	$\frac{5}{6}$	$\frac{5}{12}$	$\frac{5}{4}$	$\frac{1}{4}$	$-\frac{1}{84}$

Table 12
Closure schemes for interpolation at the c-mesh for point $i = 1/2$. Scheme 'c14i' is not presented because it is singular when $kh = \pi$.

Order	Name	$\alpha_{i1/2}$	$\alpha_{i3/2}$	a_{i0}	a_{i1}	a_{i2}	a_{i3}	a_{i4}
4	c14e	1		$\frac{5}{16}$	$\frac{15}{16}$	$-\frac{5}{16}$	$\frac{1}{16}$	
5	c15i	1	$\frac{5}{3}$	$\frac{5}{24}$	$\frac{15}{8}$	$\frac{5}{8}$	$-\frac{1}{24}$	
6	c16i	1	$\frac{7}{3}$	$\frac{35}{192}$	$\frac{35}{16}$	$\frac{35}{32}$	$-\frac{7}{48}$	$\frac{1}{6}$

For $N = 40$ there is little difference between the non-characteristic formulations. When the pulse becomes better resolved, however, the boundary schemes become relatively more important, so the formulation that does not account for p at the boundary performs best. The characteristic formulation also performs well for short times, but it becomes unstable for this problem. This will be predicted by the stability analysis in Section 3.3.

The formulation using the extrapolation also performs well in this case, which is surprising since it is arguably the least physically justified. The result shown is for a third-order explicit extrapolation scheme. It is noteworthy that when a fourth-order scheme is used for extrapolation, the solution actually degrades, and the error is close to that of the conservation condition (case 3).

The second case we consider is the one in which the value of the variable at the c-mesh is determined at the boundary. If the boundary point is not defined, there is no standard way to enforce the boundary condition in this case. Boersma [4], for example, interpolates (and extrapolates to the boundary point) the data from the

Table 13
Closure schemes for the first-derivative at the h-mesh for point $i = 0$.

Order	Name	α_{i0}	α_{i1}	a_{i0}	$a_{i1/2}$	$a_{i3/2}$	$a_{i5/2}$	$a_{i7/2}$	$a_{i9/2}$
3	h03ea	1		$-\frac{46}{15}$	$\frac{15}{4}$	$-\frac{5}{6}$	$\frac{3}{20}$		
4	h04ea	1		$-\frac{352}{105}$	$\frac{35}{8}$	$-\frac{35}{24}$	$\frac{21}{40}$	$-\frac{5}{56}$	
4	h04ia	1	15	$-\frac{16}{15}$	-15	$\frac{50}{3}$	$-\frac{3}{5}$		
5	h05ia	1	-105	$-\frac{2032}{105}$	140	$-\frac{385}{3}$	$\frac{42}{5}$	$-\frac{5}{7}$	
6	h06ia	1	$-\frac{945}{37}$	$-\frac{86,392}{105}$	$-\frac{22,365}{11,655}$	$-\frac{4865}{148}$	$\frac{4357}{1480}$	$-\frac{495}{1036}$	$\frac{245}{5328}$
3	h03eb	1			$-\frac{71}{24}$	$\frac{47}{8}$	$-\frac{31}{8}$	$\frac{23}{24}$	
4	h04eb	1			$-\frac{31}{8}$	$\frac{229}{24}$	$-\frac{75}{8}$	$\frac{37}{8}$	$-\frac{11}{12}$
3	h03ib	1	23		-25	26	-1		
4	h04ib	1	22		$-\frac{577}{24}$	$\frac{201}{8}$	$-\frac{9}{8}$	$\frac{1}{24}$	
5	h05ib	1	$\frac{1689}{71}$		$-\frac{14,587}{568}$	$\frac{11,243}{426}$	$-\frac{129}{284}$	$-\frac{47}{142}$	$-\frac{127}{1704}$

Table 14
Closure schemes for the first-derivative at the h-mesh for point $i = 1$.

Order	Name	α_{i0}	α_{i1}	α_{i2}	a_{i0}	$a_{i1/2}$	$a_{i3/2}$	$a_{i5/2}$	$a_{i7/2}$	$a_{i9/2}$
4	h14i	$\frac{1}{22}$	1	$\frac{1}{22}$		$-\frac{12}{11}$	$\frac{12}{11}$			
5	h15ia	$-\frac{2}{75}$	1	$\frac{1}{5}$	$\frac{272}{1125}$	$-\frac{7}{5}$	$\frac{46}{45}$	$\frac{17}{125}$		
6	h16ia	$-\frac{3}{70}$	1	$\frac{7}{18}$	$\frac{1088}{3675}$	$-\frac{79}{54}$	$\frac{5}{6}$	$\frac{17}{50}$	$-\frac{17}{2646}$	
5	h15ib	$\frac{1}{22}$	1	$-\frac{127}{198}$		$-\frac{665}{594}$	$\frac{41}{22}$	$-\frac{17}{22}$	$\frac{17}{594}$	
6	h16ib	$\frac{9}{62}$	1	$-\frac{10,799}{558}$		$-\frac{1913}{837}$	$\frac{4439}{186}$	$-\frac{1411}{62}$	$\frac{2125}{1674}$	$-\frac{17}{186}$

Table 15
Closure schemes for the first-derivative at the c-mesh for point $i = 0$.

Order	Name	α_{i0}	$\alpha_{i1/2}$	a_{i0}	a_{i1}	a_{i2}	a_{i3}	a_{i4}	a_{i5}
3	c03ea	1		$-\frac{11}{6}$	3	$-\frac{3}{2}$	$\frac{1}{3}$		
4	c04ea	1		$-\frac{25}{12}$	4	-3	$\frac{4}{3}$	$-\frac{1}{4}$	
5	c05ea	1		$-\frac{137}{60}$	5	-5	$\frac{10}{3}$	$-\frac{5}{4}$	$\frac{1}{5}$
4	c04ia	1	6	$-\frac{91}{12}$	$\frac{33}{4}$	$-\frac{3}{4}$	$\frac{1}{12}$		
5	c05ia	1	$\frac{384}{71}$	$-\frac{5999}{852}$	$\frac{556}{71}$	$-\frac{69}{71}$	$\frac{44}{213}$	$-\frac{7}{285}$	
6	c06ia	1	$\frac{160}{31}$	$-\frac{3173}{465}$	$\frac{955}{124}$	$-\frac{215}{186}$	$\frac{65}{186}$	$-\frac{5}{62}$	$\frac{17}{1860}$

Table 16
Closure schemes for the first-derivative at the c-mesh for point $i = 1/2$.

Order	Name	α_{i0}	$\alpha_{i1/2}$	$\alpha_{i3/2}$	a_{i0}	a_{i1}	a_{i2}	a_{i3}	a_{i4}	a_{i5}
3	c13e		1		$-\frac{23}{24}$	$\frac{7}{8}$	$\frac{1}{8}$	$-\frac{1}{24}$		
4	c14e		1		$-\frac{11}{12}$	$\frac{17}{24}$	$\frac{3}{8}$	$-\frac{5}{24}$	$\frac{1}{24}$	
4	c14ia	$\frac{1}{6}$	1	$\frac{1}{3}$	$-\frac{5}{4}$	1	$\frac{1}{4}$			
5	c15ia	$\frac{1}{6}$	1	$\frac{7}{9}$	$-\frac{133}{108}$	$\frac{1}{2}$	$\frac{3}{4}$	$-\frac{1}{54}$		
6	c16ia	$\frac{9}{64}$	1	$\frac{17}{9}$	$-\frac{7817}{6912}$	$-\frac{41}{48}$	$\frac{133}{64}$	$-\frac{43}{432}$	$\frac{5}{78}$	
5	c15ib		1	$\frac{71}{9}$	$-\frac{127}{216}$	$-\frac{49}{6}$	$\frac{37}{4}$	$-\frac{29}{54}$	$\frac{1}{24}$	
6	c16ib		1	$\frac{62}{9}$	$-\frac{10,799}{17,280}$	$-\frac{2713}{384}$	$\frac{523}{64}$	$-\frac{937}{1728}$	$\frac{25}{384}$	$-\frac{3}{640}$

c-mesh to the h-mesh, enforces the boundary condition, and then interpolates back, modifying all the values in the domain. On the other hand, if the extra point is considered, the boundary condition can be applied naturally in the same way as in the previous case (because the data at the boundary is included in the formulation). Note that, for this case, we can consider a conservative or a characteristic treatment for the boundary value of u. Summarizing, the cases tested are:

1. p is not considered explicitly at the boundary. The boundary condition is imposed through extrapolation and interpolation after each time step as in Boersma [4]. u is marched using the original Eq. (10).
2. p is considered explicitly at the boundary. u is marched using (10), the original equation.
3. Same as case 2, but u is marched using (11), the characteristic equation.

The results for the same test as before are shown in Fig. 13.

In this case, the procedure of extrapolation and interpolation leads to significantly greater errors, especially when $N = 40$. This can be understood if we consider that in the $N = 40$ case the components of the high frequency modes is higher, and that the interpolation operator introduces damping, especially in the high frequency modes. The non-characteristic formulation with extra point performs better in this case, and the characteristic one performs well if the problem is well resolved.

Finally, the last test considered is the one in which u is set to zero in one end, and a characteristic non-reflecting condition is set in the other end. Results are shown in Fig. 14 for $N = 40$ and $N = 200$ for two sets of boundary schemes. It is seen that the characteristic boundary treatment is effective in removing energy from the domain. The formulation is unstable (as before) and this is noted when the norm increases slowly as t gets higher.

3.3. Stability analysis

To analyze stability, the system of equations is expressed in matrix form as $\boldsymbol{V}_t = \mathbf{A}\boldsymbol{V} + \boldsymbol{b}$, where $\boldsymbol{V}_t$ is the time-derivative of $\boldsymbol{V}$ and $\boldsymbol{b}$ is a vector which accounts for the boundary conditions. The eigenvalues of the spatial operator matrix $\mathbf{A}$ are computed. If there are eigenvalues with positive real part, the system is asymptotically unstable.

For the solution of the ME1, the cases with higher-order closures for the derivative were found to be stable when fourth-order schemes are used for interpolation for the near-boundary point, as in the test cases of Tables 6 and 7.

For the ME2, Fig. 15 shows the eigenvalues of the stability analysis when Dirichlet conditions are applied on u at both boundaries. The formulations which do not use characteristic equations for the boundary points (Fig. 15a) lead to pure imaginary eigenvalues and

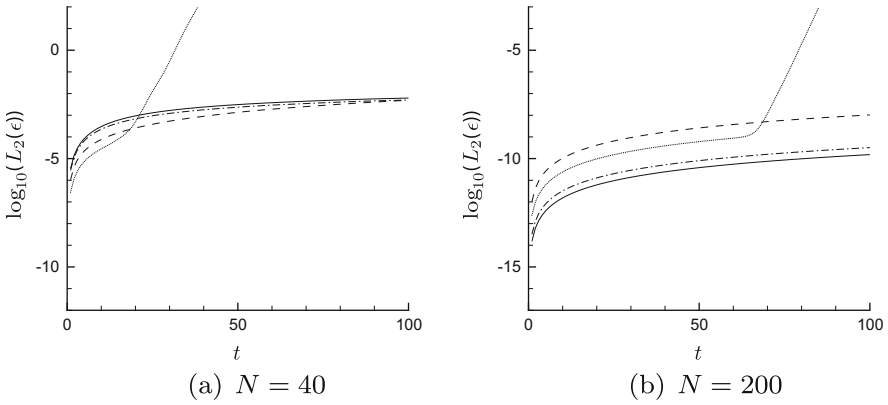

Fig. 12. Error in the marched solution as a function of time when Dirichlet condition is specified in the u variable, for (a) $N = 40$ and (b) $N = 200$ for the cases 1 —, 2 -·-, 3 ---- and 4 ·····.

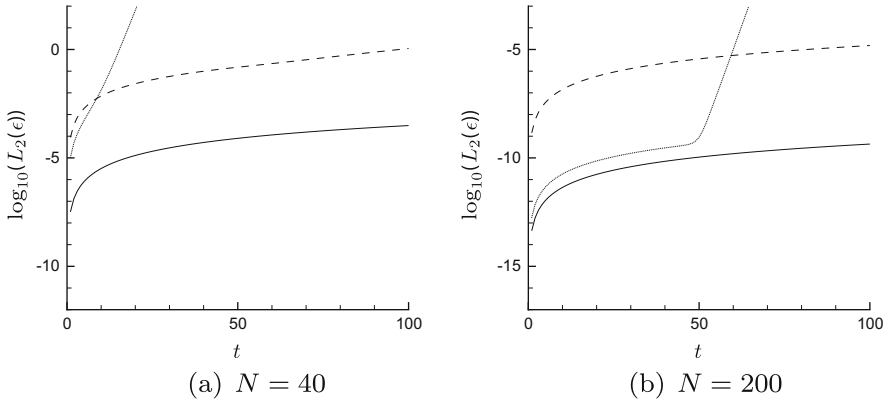

Fig. 13. Error in the marched solution as a function of time when Dirichlet condition is specified in the p variable, for (a) $N = 40$ and (b) $N = 200$ for the cases 1 —, 2 ---- and 3 ·····.

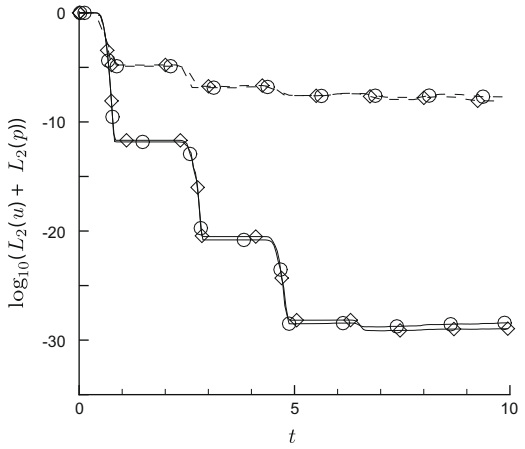

Fig. 14. Energy left in the computational domain as a function of time for model Eq. (2). A Dirichlet condition is imposed at the left boundary on u, and a non-reflecting condition is set at the right, for $N = 40$ ----, and $N = 200$ —, for the closure cases in Table 8: ♦, 1a; ○, 2a.

hence a stable system when any of the closures of Table 8 are used, both in the cases in which we consider and we do not consider the boundary point in the c-mesh. Note that these include schemes of order four for the boundary point and five for the near-boundary one. The use of closures of order higher than those usually makes the system unstable. Similar results are obtained when p is imposed at the boundary.

On the other hand, the characteristic formulation has many eigenvalues with positive real part, making that formulation unstable (Fig. 15b). However, the real part is small in comparison to the imaginary part, and hence a relatively small growth rate can be expected in time. It is also possible to stabilize the system by choosing the value of the CFL number and making all the eigenvalues fall in the stable region of the RK4 method. This has been done in tests which are not presented here, but this approach is not generally useful. It is also shown in the figure that a stabilizing effect of a viscous term of the form $(\nu\partial_{xx}u)$ has on the system. The eigenvalues presented are for ν values of 0, 1/20,000 and 1/10,000.

This stability result is confirmed when the problem is marched in time using an RK4 scheme. In Fig. 16 the evolution of the L_2 norm for different values of viscosity is shown. It is seen that the simulation is stable for $\nu = 1/10{,}000$ but unstable for $\nu = 0$ and $\nu = 1/20{,}000$.

4. Navier–Stokes test cases

The stable combination of fourth- and fifth-order boundary schemes is implemented in a Navier–Stokes code in two dimensions, with the boundary conditions treated with the NSCBC method [8].

Implementation in dimensions higher than one requires an additional but straightforward procedure for the boundary-parallel components of the mass-flux. Starting from a regular uniform mesh (cc-mesh), we define a mesh staggered in x (hc-mesh), a mesh staggered in y (ch-mesh) and a mesh staggered in both x

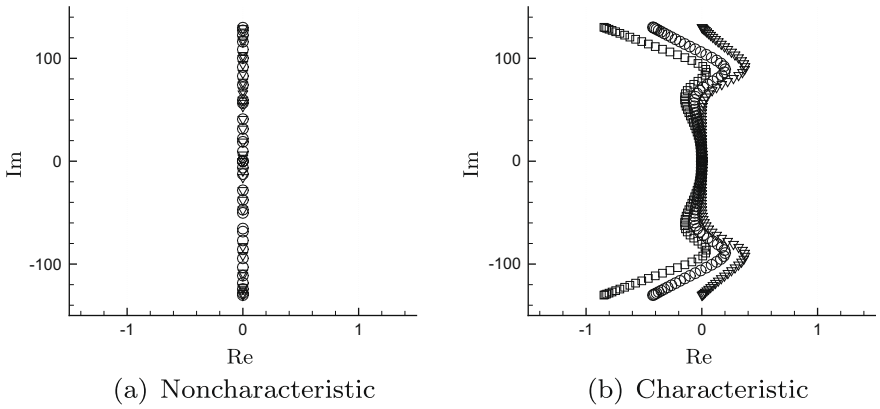

Fig. 15. Eigenvalues for the model Eq. (2) when Dirichlet boundary conditions in u are imposed in (a) non-characteristic and (b) characteristic form. References: In (a), $v = 0$ for closures: ∇,3b; ∘, 2a. In (b), closure 2b with: ∇, $v = 0$; ∘, $v = 1/20{,}000$; □, $v = 1/10{,}000$.

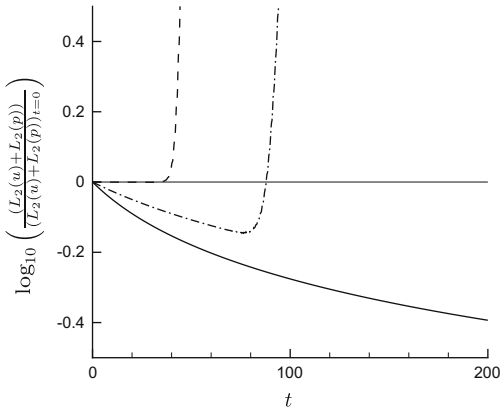

Fig. 16. Normalized L_2 norm of the time marched solution for model Eq. (2) with a viscous term in u, when Dirichlet boundary conditions in u are imposed in characteristic form. References: closure 2b with: $v = 0$ (----); $v = 1/20{,}000$ (-·-); $v = 1/10{,}000$ (—).

and y (hh-mesh). The variables ρ and E are as in one dimension on the cc-mesh, m_x on the hc-mesh, and m_y on the ch-mesh (Fig. 17), where it is seen that an additional extra point was added to define m_x (for this boundary orientation) at the boundary as well. Otherwise the implementation is as in one dimension.

To illustrate how the present approach can be used to treat boundary conditions in Navier–Stokes problems, a channel flow

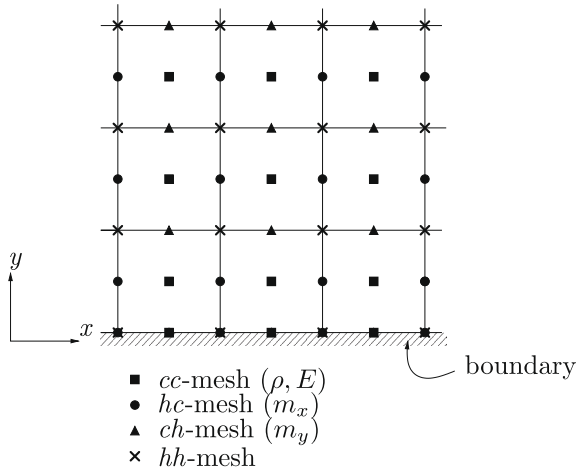

Fig. 17. Staggered mesh in two dimensions.

is simulated. This example involves inflow, outflow and wall boundary conditions. The parameters used are the same as those in Poinsot and Lele [8]. For completeness, these parameters are reproduced below. The channel has width $2l$ and length $L = 10l$. The inflow conditions at $x = 0$ are given by

$$u(0,y,t) = u_0\left(\cos\left(\frac{\pi}{2}\frac{y}{l}\right)\right)^2,$$
$$v(0,y,t) = 0,$$
$$T(0,y,t) = T_0,$$

where u, v are the x and y component of the velocity and T is the temperature. The boundary condition at $x = L$ is a non-reflecting outflow, with $\sigma = 0.25$. The channel has isothermal no-slip lateral walls, with $T = T_0$. The Reynolds number and the Mach number are $\mathrm{Re} = u_0 l/v = 15$ ($\mathrm{Re}_{a_0} = a_0 l/v = 150$) and $u_0/c = 0.1$. A mesh of 121×81 points was used.

The resulting pressure, velocity and temperature fields are shown in Fig. 18, where it is seen that good agreement is obtained with the numerical solutions presented in Poinsot and Lele [8].

As a second example we present the results of a simulation of Tollmien–Schlichting (TS) waves in a boundary layer with a free stream Mach number of 0.088. A similar test was reported by Nagarajan [10], and compared with the theoretical results obtained by Gaster [11] and with the simulation results by Fasel and Konzelmann [12]. The setup and set of parameters is similar to that used in Nagarajan [10]: a grid of 400×300 points was used, being the grid in x uniform with $\mathrm{Re}_{\Delta x} = 1000$, and the grid in y refined close to the wall. In the y-direction, the domain extends to $H/\delta_i = 165$, being H the distance from the wall, and δ_i the displacement thickness at the inflow ($Re_x = 15{,}000$). The boundary conditions at the wall, including the suction and blowing "patch", are implemented using the NSCBC method [8]. The parameters of the patch are all the same as in Nagarajan [10]: the velocity normal to the wall is defined by $v = A f(x)\sin(\omega t)$ between $x_1 \leqslant x \leqslant x_2$, with $Re_{x_1} = 90{,}000$ and $Re_{x_2} = 110{,}000$, and with $A = 2 \times 10^{-4} U_\infty$ the amplitude, $\omega = F U_\infty^2 Re_\infty$ the non-dimensional frequency, $F = 0.00014$, $Re_\infty = 2395$, and $f(x)$ the variation of amplitude in x,

$$f(x) = 15.1875\xi^5 - 35.4375\xi^4 + 20.25\xi^3$$
$$\xi(x) = \begin{cases} \left(\frac{x - x_1}{x_m - x_1}\right)^3 & x_1 \leqslant x \leqslant x_m \\ \left(\frac{x_2 - x}{x_2 - x_m}\right)^3 & x_m \leqslant x \leqslant x_2 \end{cases}$$

For this problem, an eighth-order, high-resolution filter was used in the x-direction only, to avoid the growth of numerical instabilities, apparently caused by the difference in grid spacing

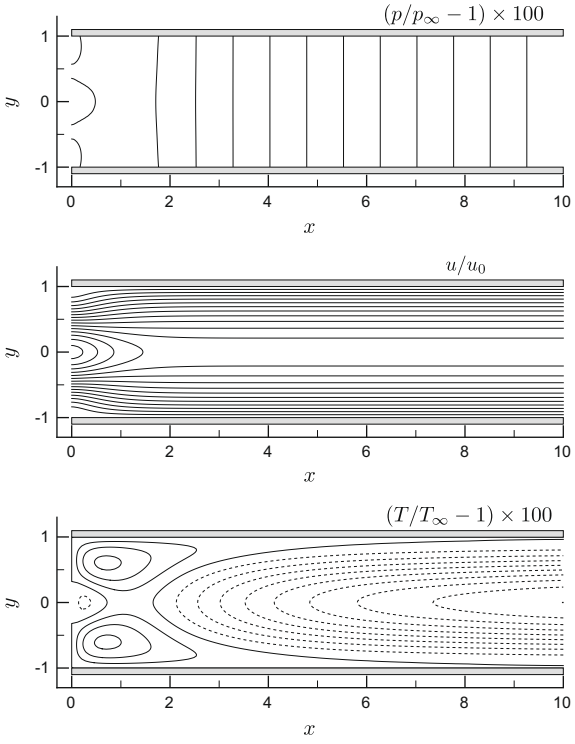

Fig. 18. Contours of: $(p/p_\infty - 1) \times 100$, 12 levels from 1.270 to 2.435; u/u_0, 16 levels from 0 to 1; $(T/T_\infty - 1) \times 100$, 13 levels from −0.075 to 0.025. Negative contours are dashed.

between the x- and y-directions. The details of this high-order filter are reported by Topalian [13]. The growth rate of the instability wave and the u- and v-velocity eigenvectors at $\mathrm{Re}_{\delta^*} = 600$ are compared to the DNS results in Fasel and Konzelmann [12] (Fig. 19), where it is seen that good agreement is obtained.

As it was mentioned by Nagarajan [10], this problem is very sensitive to the grid resolution near the wall, specifically in the computation of the amplitude of the kinetic energy integral. It is reported [10] that 10 points in the momentum thickness at the inflow were used for a fourth-order set of boundary schemes, and boundary conditions were implemented indirectly, without the use of extra points. For the present simulation 7 points per momentum thickness were sufficient to match the converged results of Nagarajan [10].

A third test case is a field of Taylor–Green vortices entering and leaving the domain via inflow and outflow boundary conditions, convected by a $M = V_0/a_0 = 0.25$ subsonic flow. This example illustrates the applicability of the proposed boundary scheme for cases with inflow and outflow turbulent flow. The initial velocity field is given by

$$u(x,y) = u' \sin(kx)\cos(ky)$$
$$v(x,y) = V_0 - v' \cos(kx)\sin(ky)$$

with $V_0 = 0.25$, $u' = v' = 0.05$, and $k = 4\pi/L$. The domain length is set to $L = 1$ in both directions, being the x-direction periodic. As the flow evolves in time, the vortices enter the domain from $y = 0$. The Reynolds number is set to $\mathrm{Re} = \frac{LV_0}{\nu} = 5000$. At the outflow, the approximately non-reflecting NSCBC boundary condition is used, with $\sigma = 0.25$ [8]. Fig. 20 shows a snapshot of vorticity after fifteen flow through times ($t_f = L/V_0$), and the evolution of the L_2 norm of vorticity in the domain. It is seen that little distortion is apparent at the inflow and outflow. Also, that the L_2 norm remains bounded, following a small change after the initial transient, and continues with small-amplitude oscillation in time (less than 0.5%), that are product of the partial reflections at the outflow and inflow. This shows that the proposed boundary conditions and schemes are stable and suitable for this type of problems. It is worth noting that for applications when acoustic effects are important, a boundary treatment that combines this inflow/outflow conditions with buffer zones is better suited [14].

Further examples using these boundary treatments are reported elsewhere [13,15].

5. Conclusions

In this work, we have tested staggered mesh discretization with all the variables at the boundary to facilitate the application of boundary conditions. Tests show that resolution is not hurt by the use of this extra-point on the c-mesh. Furthermore the one-dimensional test cases show that good results are obtained also when the problem is marched in time. When a Dirichlet condition is imposed in the variable on the c-mesh, the use of the interpolation and extrapolation process as in Boersma [4] leads to higher errors. It is clearly better to define the boundary point and apply the Dirichlet condition to it. The implementation of boundary conditions in characteristic form (as by Poinsot and Lele [8]) is also explored. This has the advantage of giving physically meaningful values to all the variables. This strategy is more complicated than existing approaches, but not excessively, and leads generally to

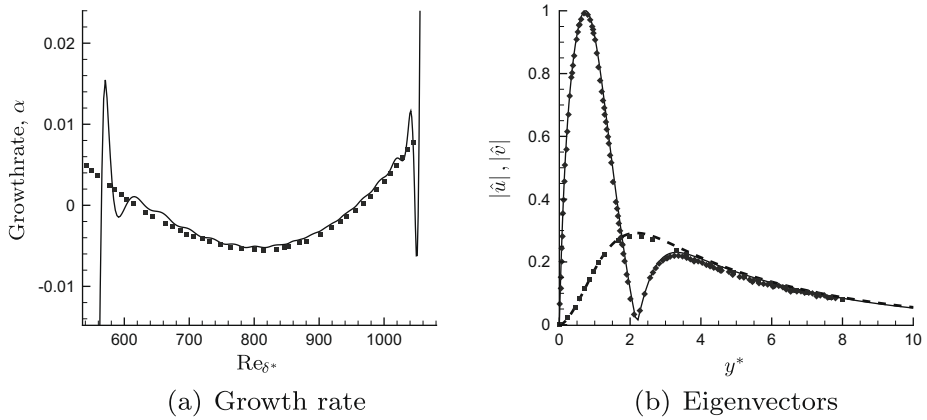

Fig. 19. Test case: Growth of Tollmien–Schlichting waves in a boundary layer. (a) — growth rate, (b) modulus of — u, and ---- v, eigenvectors at $\mathrm{Re}_{\delta^*} = 600$. Symbols are results from Fasel and Konzelmann [12].

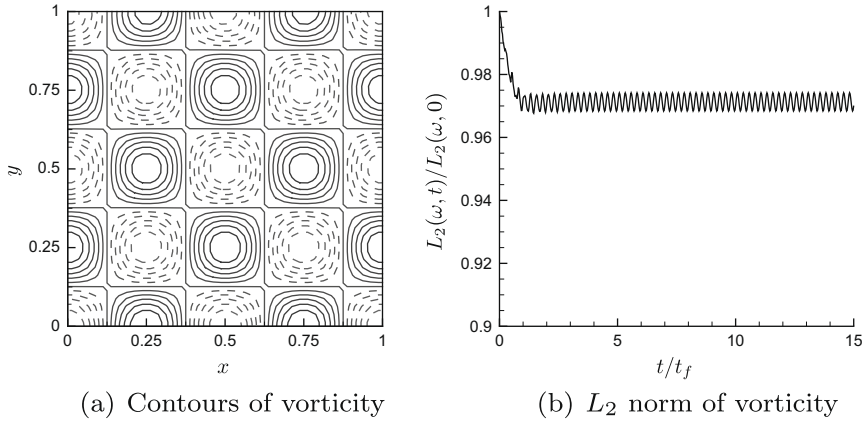

Fig. 20. Test case: Inflow/outflow of Taylor–Green vortices. (a) Contours of vorticity after 15 flow through times (negative contours are dashed), (b) L_2 norm of the vorticity field as a function of flow through times.

improved results. It can be mildly unstable, but is stabilized by very low levels of physical viscosity.

It was also shown that it is possible to use a combination of fourth and fifth-order boundary schemes to close the operators which use sixth-order implicit schemes as interior stencil. They are stable and they improve the accuracy of the solution over lower-order closures, especially as the problem becomes better resolved.

Finally, Navier–Stokes solutions in two-dimensions were shown. The extension to three-dimensions should pose no additional problem, nor should other generalizations like the treatment of time dependent boundary variables or the addition of species and reacting flow [4].

Acknowledgments

The support from the DOE – Center for Simulation of Advanced Rockets (CSAR) at UIUC for this work is gratefully acknowledged. The use of the Turing cluster maintained and operated by the Computational Science and Engineering Program at the University of Illinois is also gratefully acknowledged.

References

[1] Harlow FH, Welch JE. Numerical calculation of time-dependent viscous incompressible flow of fluid with free surface. Phys Fluids 1965;8:2182–9.
[2] Morinishi Y, Lund TS, Vasilyev OV, Moin P. Fully conservative higher order finite difference schemes for incompressible flow. J Comput Phys 1998;143(1):90–124.
[3] Lele SK. Compact finite difference schemes with spectral-like resolution. J Comput Phys 1992;103(1):16–42.
[4] Boersma BJ. A staggered compact finite difference formulation for the compressible Navier–Stokes equations. J Comput Phys 2005;208(2):675–90.
[5] Nagarajan S, Lele SK, Ferziger JH. A robust high-order compact method for large eddy simulation. J Comput Phys 2003;191(2):392–419.
[6] Tam CK, Webb J. Dispersion-relation-preserving finite difference schemes for computational acoustics. J Comput Phys 1993;107(2):262–81.
[7] Kwok WY, Moser RD, Jimnez J. A critical evaluation of the resolution properties of B-spline and compact finite difference methods. J Comput Phys 2001;174(2):510–51.
[8] Poinsot T, Lele SK. Boundary conditions for direct simulation of compressible viscous flows. J Comput Phys 1992;101(1):104–29.
[9] Colonius T. Numerically nonreflecting boundary and interface conditions for compressible flow and aeroacoustic computations. AIAA J 1997;35(7):1126–33.
[10] Nagarajan S. Leading edge effects in bypass transition. Ph.D. thesis, Stanford University; 2004.
[11] Gaster M. On the effects of boundary-layer growth on flow stability. J Fluid Mech 1974;66:465–80.
[12] Fasel H, Konzelmann U. Non-parallel stability of a flat-plate boundary layer using the complete Navier–Stokes equations. J Fluid Mech 1990;221:311–47.
[13] Topalian VD. Acoustic resonances in ducted jet systems. Ph.D. thesis, University of Illinois at Urbana–Champaign (2009).
[14] Freund JB. Proposed infow/outfow boundary condition for direct computation of aerodynamic sound. AIAA J 1997;35(4):740–2.
[15] Daimon Y, Jackson TL, Topalian V, Freund J, Buckmaster J. Acoustics in a two-dimensional slab rocket motor. In: 46th AIAA aerospace sciences meeting and exhibit, AIAA; 2008.